

# Nonlinear Conduction by Melting of Stripe-Type Charge Order in Organic Conductors with Triangular Lattices

Yasuhiro TANAKA\* and Kenji YONEMITSU

*Institute for Molecular Science, Okazaki, Aichi 444-8585, Japan*

*Department of Functional Molecular Science, Graduate University for Advanced Studies, Okazaki, Aichi 444-8585, Japan*

*JST, CREST, Tokyo 102-0075, Japan*

We theoretically discuss the mechanism for the peculiar nonlinear conduction in quasi-two-dimensional organic conductors  $\theta$ -(BEDT-TTF)<sub>2</sub>X [BEDT-TTF=bis(ethylenedithio)tetrathiafulvalene] through the melting of stripe-type charge order. An extended Peierls-Hubbard model attached to metallic electrodes is investigated by a nonequilibrium Green's function technique. A novel current-voltage characteristic appears in a coexistent state of stripe-type and nonstripe 3-fold charge orders, where the applied bias melts mainly the stripe-type charge order through the reduction of lattice distortion, whereas the 3-fold charge order survives. These contrastive responses of the two different charge orders are consistent with the experimental observations.

**KEYWORDS:** nonlinear conduction, charge order, nonequilibrium Green's function, organic conductor

Nonlinear conduction in low-dimensional electron systems has been of great interest from the viewpoint of fundamental nonequilibrium physics and possible applications to electronic devices. A well-known example is a sliding of density waves in quasi-one-dimensional materials, where a nesting of the Fermi surface is responsible for their ground states.<sup>1)</sup> In strongly correlated systems such as Mott insulators<sup>2)</sup> and charge-ordered states of transition metal oxides,<sup>3)</sup> dielectric breakdown phenomena have been observed. In one dimension, a breakdown of Mott insulators by the Landau-Zener tunneling mechanism has been proposed theoretically<sup>4)</sup> and the relevance to experimental findings has been discussed so far.

The observations of giant nonlinear conduction and spontaneous current oscillation in the organic compounds  $\theta$ -(BEDT-TTF)<sub>2</sub>CsM(SCN)<sub>4</sub><sup>5,6)</sup> ( $M$ =Co and Zn) have renewed interest since their mechanism and the electric-field-induced behaviors seem to differ in many respects from those in the above materials. The family of organic conductors  $\theta$ -(ET)<sub>2</sub>X (ET is the abbreviation of BEDT-TTF) is known to exhibit charge order (CO).<sup>7,8)</sup> It has a quasi-two-dimensional structure, where ET molecules form a triangular lattice in each conduction layer [Fig. 1(a)]<sup>9)</sup> with electron density at 3/4 filling (one hole per two ET molecules). In  $\theta$ -(ET)<sub>2</sub>RbZn(SCN)<sub>4</sub>, a metal-insulator transition with a structural distortion occurs at  $T_{CO} = 190$  K.<sup>9)</sup> A stripe-type arrangement of localized charges indexed by wave number  $\mathbf{q}_2 = (0, 0, 1/2)$ , which is called a horizontal CO [Fig. 1(b)], emerges below  $T_{CO}$ .<sup>10-12)</sup> In  $\theta$ -(ET)<sub>2</sub>CsM(SCN)<sub>4</sub>, on the other hand, coexistence of two different COs, the horizontal CO and a nonstripe CO indexed by  $\mathbf{q}_1 = (2/3, k, 1/3)$ , has been observed by X-ray experiments,<sup>13,14)</sup> although this compound does not show any long-range order. Several experiments suggest that the peculiar nonlinear conduction results from suppression of the horizontal CO by an electric field without destroying the nonstripe CO.<sup>5,15)</sup>

A similar nonlinear conduction and coexistence of two kinds of COs have also been observed in a rapidly cooled RbZn salt.<sup>16,17)</sup> Although nonlinear conduction has been found in other compounds,<sup>18,19)</sup> this unique feature of multiple charge modulation seems essential for the nonlinearity in  $\theta$ -type compounds.

Theoretically, the CO phenomenon in  $\theta$ -(ET)<sub>2</sub>X has been investigated from various aspects.<sup>20,21)</sup> The charge disproportionation results mainly from the long-range nature of the Coulomb interaction, whereas electron-phonon (e-ph) couplings are also important. In particular, the lattice distortion in the RbZn salt considerably stabilizes the horizontal CO.<sup>22-24)</sup> Compared with our knowledge on the ground states, nonequilibrium states induced by an external field have been poorly understood. Recently, Mori and coworkers have shown that a phenomenological equation can reproduce the observed nonlinear current-voltage characteristics in some compounds.<sup>18,19)</sup> However, the origin of nonlinear conduction is still unclear, so a microscopic theory is highly desirable.

With these in mind, we investigate nonequilibrium steady states of  $\theta$ -(ET)<sub>2</sub>X under applied bias voltages, using a model that takes account of both the long-range Coulomb interactions and e-ph couplings.<sup>22-24)</sup> The model describes competition among various COs, including the horizontal CO and a so-called 3-fold CO [Fig. 1(c)], the latter has a nonstripe charge pattern<sup>25)</sup> and can be related to the CO with  $\mathbf{q}_1$  in the CsM salt. The state with the horizontal CO is insulating, whereas that with the 3-fold CO is metallic.<sup>26)</sup> We show that when these two states coexist, the bias voltage melts the horizontal CO and largely alters the conduction behavior. The lattice distortion, which induces the horizontal charge modulation, has a key role in determining whether the system becomes resistive or conductive.

We consider the extended Peierls-Hubbard model<sup>22-24)</sup>

\*E-mail address: yasuhiro@ims.ac.jp

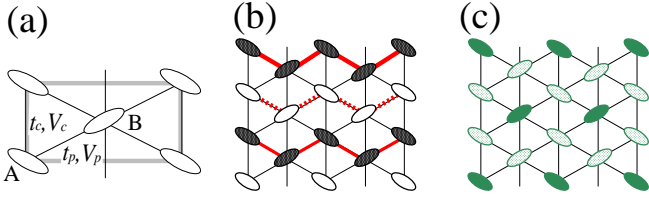


**Fig. 1.** (Color online). (a) Schematic view of the high-temperature structure for  $\theta$ -(ET)<sub>2</sub>X. Ellipses represent ET molecules. The gray rectangle shows a unit cell in which sites are labeled A and B. (b) Horizontal CO and (c) 3-fold CO, where the solid (open or shaded) ellipses denote hole-rich (-poor) molecules. In (b), the lattice distortion along the horizontal stripe is shown by the thick and broken lines.

written as

$$\begin{aligned}
 H &= \sum_{\langle ij \rangle \sigma} \left[ (t_{i,j} + \alpha_{i,j} u_{i,j}) c_{i\sigma}^\dagger c_{j\sigma} + \text{h.c.} \right] \\
 &+ U \sum_i (n_{i\uparrow} - N_e/2)(n_{i\downarrow} - N_e/2) \\
 &+ \sum_{\langle\langle ij \rangle\rangle} V_{i,j} (n_i - N_e)(n_j - N_e) + \sum_{\langle ij \rangle} \frac{K_{i,j}}{2} u_{i,j}^2, \quad (1)
 \end{aligned}$$

where  $\langle ij \rangle$  represents the summation over pairs of neighboring sites,  $c_{i\sigma}^\dagger (c_{i\sigma})$  denotes the creation (annihilation) operator for an electron with spin  $\sigma$  at the  $i$ th site,  $n_{i\sigma} = c_{i\sigma}^\dagger c_{i\sigma}$ ,  $n_i = n_{i\uparrow} + n_{i\downarrow}$ , and the averaged electron density  $N_e = 1.5$ .  $t_{i,j}$  denotes the transfer integrals and  $U$  the on-site repulsion. For the intersite Coulomb interactions  $V_{i,j}$ , we consider up to third-neighbor pairs of sites, the summation over which is represented by  $\langle\langle ij \rangle\rangle$ . The e-ph coupling constant, the lattice displacement and the elastic constant are denoted by  $\alpha_{i,j}$ ,  $u_{i,j}$ , and  $K_{i,j}$ , respectively. We introduce new variables as  $y_{i,j} = \alpha_{i,j} u_{i,j}$  and  $s_{i,j} = \alpha_{i,j}^2 / K_{i,j}$ .<sup>22-24</sup>

The structure of  $\theta$ -(ET)<sub>2</sub>X in the high-temperature metallic phase is shown in Fig. 1(a). There are two transfer integrals  $t_c$  and  $t_p$  on the vertical and diagonal bonds, respectively. We set  $t_c = -0.04$  (eV) and  $t_p = 0.1$  in the following. On the vertical (diagonal) bonds, we define the nearest-neighbor interaction  $V_c$  ( $V_p$ ). For the second- and third-neighbor interactions, we write them as  $V_{i,j} = V_{lr}/r_{ij}$ . Here,  $r_{ij}$  is the distance between the  $i$ th and  $j$ th sites. The horizontal CO and the 3-fold CO are schematically shown in Figs. 1(b) and 1(c), respectively. For e-ph couplings, we consider a lattice distortion caused by the molecular rotation, which is crucial for stabilizing the horizontal CO.<sup>22-24</sup> This is because it gives homogeneous modulation in the transfer integrals along with a horizontal stripe. We denote the modulation as  $y_\phi$  and write the corresponding e-ph coupling as  $s_\phi$ . These variables are defined only on the bonds that are depicted by the thick and broken lines in Fig. 1(b). We assume that  $y_\phi$  is independent of bond index so that the transfer integrals on the hole-rich (-poor) stripe are written as  $t_p + y_\phi$  ( $t_p - y_\phi$ ) with  $y_\phi > 0$ . The elastic energy for each distorted bond is given by  $y_\phi^2 / (2s_\phi)$ . For simplicity, we do not take account of other types of modulation.<sup>22-24</sup>

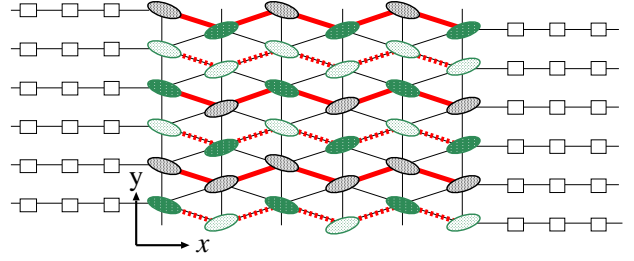


**Fig. 2.** (Color online). Schematic picture of the model. The left and right electrodes are attached to the central part where the horizontal and 3-fold COs coexist when the bias voltage is absent. A horizontal charge modulation induced by the lattice distortion on the 3-fold charge pattern is represented by the gray ellipses on the thick bonds. The  $x$ -axis ( $y$ -axis) is along (perpendicular to) the conduction direction.

We describe the steady states under applied bias voltages by the nonequilibrium Green's function method.<sup>27,28</sup> As shown in Fig. 2, we attach the left and right ( $\alpha = L, R$ ) semi-infinite metallic electrodes to the central part that is described by eq. (1). A coexistent CO, which will be discussed later, is realized in the absence of the bias voltage. For the  $i$ th site [ $i = (i_x, i_y)$ ] in the central part, we define its coordinates as  $(i_x, i_y)$  if  $i_x$  is odd, and  $(i_x, i_y - 1/2)$  if  $i_x$  is even. The numbers of sites are denoted by  $L_x$  and  $L_y$  ( $1 \leq i_x \leq L_x$  and  $1 \leq i_y \leq L_y$ ). We assume that electrons in the leads are noninteracting and that they move only in the  $x$ -direction; for simplicity, the electrodes are one-dimensional. The effects of the leads on the central part are incorporated into the self-energies. In the wide-band limit, the retarded self-energies are independent of energy and written as  $(\Sigma_\alpha^r)_{ij} = -\frac{i}{2} \gamma_\alpha \sum_{i_\alpha} \delta_{ii_\alpha} \delta_{ji_\alpha}$ , where  $\delta_{ij}$  is the Kronecker delta,  $i_L$  ( $i_R$ ) denotes the site that is connected with the left (right) electrode, and  $\gamma_\alpha$  the coupling constant between the central part and the electrode  $\alpha$ .

We use the Hartree-Fock approximation for the  $U$ ,  $V_p$ , and  $V_c$  terms in eq. (1). For the second- and third-neighbor interactions, we employ the Hartree approximation. These interactions contribute to a redistribution of charges near the electrodes,<sup>28</sup> whereas the charge disproportionation is mainly caused by  $V_p$  and  $V_c$ . We consider the case of  $V_p, V_c \gg V_{lr}$ . The periodic boundary condition is adopted along the  $y$ -axis. In the mean-field Hamiltonian, we introduce a scalar potential  $\psi$  that is defined by the Hartree terms for the intersite Coulomb interactions as  $\psi(i_x, i_y) = \sum_{j \neq i} V_{i,j} (\langle n_j \rangle - N_e) + a i_x + b$ , which is equivalent to the Poisson equation.<sup>27</sup> The slope of the potential,  $a i_x$ , describes the electric field in the central part.<sup>28</sup> The constants  $a$  and  $b$  are so determined that  $\psi$  satisfies the boundary conditions,  $\frac{1}{L_y} \sum_{i_y} \psi(1, i_y) = V/2$  and  $\frac{1}{L_y} \sum_{i_y} \psi(L_x, i_y) = -V/2$ , when the bias voltage  $V$  is applied to the system. We assume that the work-function differences at the interfaces are absent.

The steady states under the applied bias are obtained as a self-consistent solution for the mean fields that are calculated by the method described in ref. 27. The electron density  $\langle n_{i\sigma} \rangle$  is calculated by decomposing it

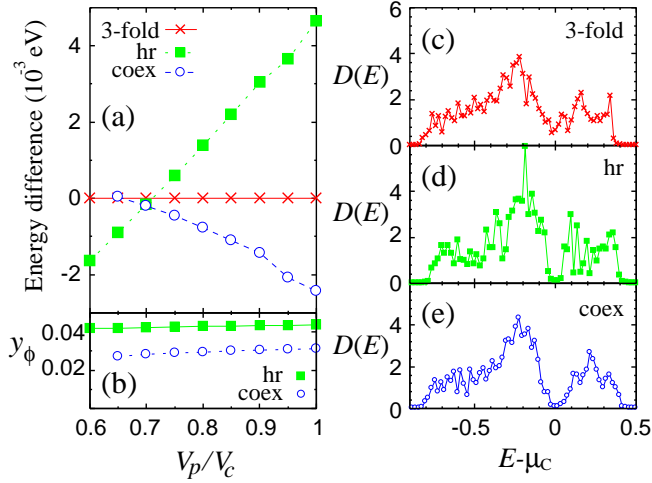


**Fig. 3.** (Color online). (a) Energies of the horizontal (hr) and coexistent (coex) COs with  $L_x = L_y = 18$ ,  $U = 0.6$ ,  $V_c/U = 0.35$ ,  $s_\phi = 0.1$ ,  $V_{lr} = 0.02$ , and  $\gamma_R = \gamma_L = 0$ , relative to that of the 3-fold CO, as a function of  $V_p/V_c$ . (b) The lattice distortions  $y_\phi$  for the horizontal and coexistent COs. Density of states for (c) the 3-fold, (d) horizontal, and (e) coexistent COs in the case of  $V_p/V_c = 1$ .

into the “equilibrium” and “nonequilibrium” parts as  $\langle n_{i\sigma} \rangle = n_i^{\text{eq}} + \sum_\alpha \delta n_{i\sigma}^\alpha$ .<sup>27)</sup> The same decomposition is used to obtain  $\langle c_{i\sigma}^\dagger c_{j\sigma} \rangle$ . We adjust the chemical potential  $\mu_C = (\mu_L + \mu_R)/2$ <sup>27)</sup> such that the electron density of the central part is fixed at  $3/4$  filling. Here,  $\mu_L$  and  $\mu_R$  are the left and right chemical potentials, respectively. For finite  $V$ , we set  $\mu_L = \mu_C + V/2$  and  $\mu_R = \mu_C - V/2$ . The lattice distortion  $y_\phi$  is determined as in the equilibrium case.<sup>22)</sup> The current  $J$  is obtained by using  $\delta n_{i\sigma}^\alpha$  as  $J = \gamma_R \sum_{iR\sigma} \delta n_{iR\sigma}^L - \gamma_L \sum_{iL\sigma} \delta n_{iL\sigma}^R$ ,<sup>27)</sup> where we set  $e = \hbar = 1$ . In the following, we use  $U = 0.6$ ,  $V_c/U = 0.35$ ,  $s_\phi = 0.1$ , and  $V_{lr} = 0.02$ . The size of the central part is  $L_x = L_y = 18$  unless otherwise noted.

First, we consider the equilibrium case where the CO system is isolated from the electrodes ( $\gamma_R = \gamma_L = 0$ ). The ground-state energies per site of three mean-field solutions as a function of  $V_p/V_c$  are shown in Fig. 3(a), where the energy of the 3-fold CO is set at zero. The horizontal and coexistent COs have a finite lattice distortion  $y_\phi$ , as shown in Fig. 3(b). For  $V_p/V_c < 0.7$ , the horizontal CO is the most stable, whereas the 3-fold CO has a lower energy than the horizontal CO for  $V_p/V_c > 0.7$ . This results from charge frustration on the triangular lattice.<sup>25,26)</sup> The 3-fold CO is further stabilized by coexisting with the  $y_\phi$ -induced horizontal CO (Fig. 2) and becomes the ground state near  $V_p/V_c = 1$ .<sup>22)</sup> For each CO pattern, we show the density of states  $D(E)$  in Figs. 3(c)-3(e) for  $V_p/V_c = 1$ , where we used a broadening factor of  $\eta = 0.01$ . A finite  $D(E)$  at the Fermi level exists for the 3-fold CO since this state is metallic,<sup>26)</sup> whereas the horizontal CO has an energy gap. In the coexistent CO,  $D(E)$  at  $E = \mu_C$  is suppressed compared with that for the 3-fold CO, which is due to the horizontal CO. However, we note that the state has no energy gap in the thermodynamic limit.<sup>22)</sup>

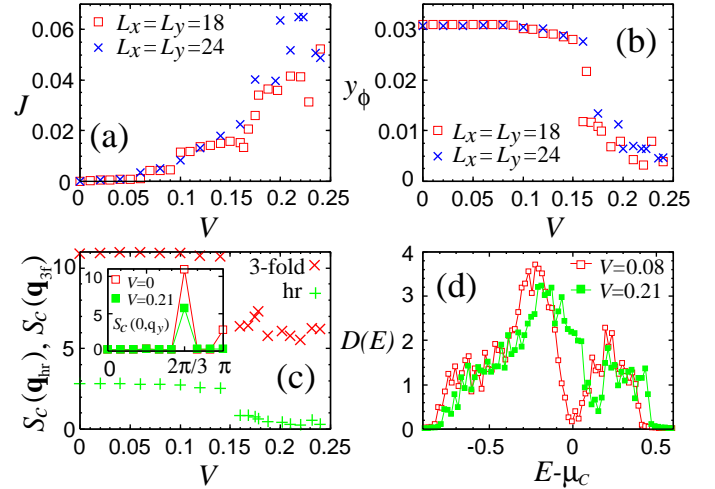


**Fig. 4.** (Color online). (a) Electric current  $J$ , (b) lattice distortion  $y_\phi$ , and (c) charge structure factors  $S_c(\mathbf{q}_{\text{hr}})$  and  $S_c(\mathbf{q}_{3f})$  as a function of  $V$ , where  $\mathbf{q}_{\text{hr}}$  and  $\mathbf{q}_{3f}$  are the wave vectors for the horizontal (hr) and 3-fold COs, respectively. In (a) and (b), results with  $L_x = L_y = 24$  are also shown. In (c), the  $q_y$  dependence of  $S_c(0, q_y)$  is shown in the inset. (d) Density of states for  $V = 0.08$  and  $0.21$ .

Next, we discuss the results obtained with finite bias  $V$ . We set  $V_p/V_c = 1$  and  $\gamma_L = \gamma_R = 0.03$ , where the ground state without the bias is the coexistent CO. The current-voltage characteristics and the distortion  $y_\phi$  are shown in Figs. 4(a) and 4(b), respectively. In these figures, we show the results with  $L_x = L_y = 24$  for comparison. The behaviors of  $J$  and  $y_\phi$  are qualitatively the same as those with  $L_x = L_y = 18$ . With increasing  $V$ , the current gradually increases and abruptly becomes large at  $V_{cr} \sim 0.17$ . For small  $V$  and  $L_x = L_y = 18$ ,  $J$  has stepwise structures owing to the finite-size effect.<sup>28)</sup> As shown in Fig. 4(b),  $y_\phi$  is almost unchanged for  $V < V_{cr}$ , although it shows a gradual decrease with increasing  $V$ . At  $V = V_{cr}$ ,  $y_\phi$  steeply decreases, which is directly related to the reduction of the horizontal CO.

The effects of bias voltages on the horizontal and 3-fold components of the charge distribution are obtained by calculating the charge structure factor, which is defined as

$$S_c(\mathbf{q}) = \frac{1}{N_s} \sum_{\mu, \nu} (\langle n_{\mu A} n_{\nu A} \rangle + \langle n_{\mu B} n_{\nu B} \rangle) e^{i\mathbf{q}(\mathbf{R}_\mu - \mathbf{R}_\nu)}. \quad (2)$$

Here, we use the unit cell shown in Fig. 1(a), which is labeled by  $\mu, \nu$ .  $A$  and  $B$  are indices for sites inside the unit cell. The position vector for the  $\mu$ -th ( $\nu$ -th) unit cell is denoted by  $\mathbf{R}_\mu$  ( $\mathbf{R}_\nu$ ) and  $N_s = L_x \times L_y$ . The wave vectors that correspond to the horizontal and 3-fold components are  $\mathbf{q}_{\text{hr}} = (0, \pi)$  and  $\mathbf{q}_{3f} = (0, 2\pi/3)$ , respectively. In Fig. 4(c), we show  $S_c(\mathbf{q}_{\text{hr}})$  and  $S_c(\mathbf{q}_{3f})$  as a function of  $V$ , and the  $q_y$  dependence of  $S_c(0, q_y)$  for  $V = 0$  and  $0.21$  in the inset. In the  $V = 0$  case,  $S_c(0, q_y)$  has two peaks at  $\mathbf{q}_{\text{hr}}$  and  $\mathbf{q}_{3f}$  since the two COs coexist. Because the 3-fold charge modulation is larger than the horizontal one, we have  $S_c(\mathbf{q}_{3f}) > S_c(\mathbf{q}_{\text{hr}})$ . For  $V < V_{cr}$ , the values of  $S_c(\mathbf{q}_{\text{hr}})$  and  $S_c(\mathbf{q}_{3f})$  are almost unchanged, which indi-

cates that the coexistent CO is robust against the applied bias. For  $V > V_{cr}$ , both  $S_c(\mathbf{q}_{hr})$  and  $S_c(\mathbf{q}_{3f})$  decrease and the charge distribution is largely modified. In particular, the horizontal component is drastically weakened. For  $V = 0.21$ , the  $\mathbf{q}_{hr}$  peak in  $S_c(0, q_y)$  disappears. Correspondingly,  $y_\phi$  becomes very small for large  $V$ . However, the 3-fold component survives even in the region  $V > V_{cr}$ . It is noteworthy that  $J$  increases without destroying the 3-fold CO. We show the density of states for  $V = 0.08$  and  $0.21$  in Fig. 4(d). For  $V = 0.08$ ,  $D(E)$  is qualitatively the same as that in the  $V = 0$  case shown in Fig. 3(e). Since the coexistent CO has no energy gap,<sup>22)</sup> a small current can flow even for  $V < V_{cr}$ . For  $V = 0.21$ , a large  $D(E)$  appears at  $E = \mu_C$  since the horizontal charge modulation is suppressed. The change in the conduction behavior is triggered by the reduction in  $y_\phi$ . If  $y_\phi$  is large, the horizontal CO persists so the system is resistive, whereas if  $y_\phi$  decreases, only the 3-fold CO remains so the system becomes conductive.

Let us discuss the relevance to experimental results on  $\theta$ -(ET)<sub>2</sub>X. Our results basically reproduce the X-ray results<sup>5,15,17)</sup> that indicate that the nonlinear conduction is caused by the melting of the horizontal CO whereas the nonstripe CO remains. In the CsZn salt, the resistivity begins to increase at around 50 K.<sup>9)</sup> This corresponds to the growth of X-ray intensity for the horizontal CO, whereas that for the nonstripe CO shows only slight temperature dependence.<sup>13,14)</sup> Theoretically, such contrastive temperature dependences of stripe-type and 3-fold-type charge fluctuations have been shown by the random phase approximation,<sup>29)</sup> where the former comes from the Fermi-surface instability assisted by e-ph couplings, whereas the latter is due to the wave-vector dependence of the Fourier transform of the intersite Coulomb interaction. These facts also suggest that the horizontal CO induced by the lattice distortion is directly related to the resistive behavior, which is consistent with our results. However, there are some issues that remain to be clarified. Experimentally, the nonlinear conduction appears in a state with no long-range CO, which is in contrast to the results of our mean-field calculations. Therefore, at present, it is difficult to compare the results quantitatively. In fact, the electric fields required for nonlinearity ( $\sim 1$  V/cm for the CsZn salt and  $\sim 10$  V/cm for the rapidly cooled RbZn salt) are much smaller than that in the present study. For a quantitative comparison, the effects of quantum fluctuations must be taken into account. The finite-size effects<sup>28)</sup> as well as the thermal fluctuations will affect the values of the threshold voltage. Recently, an inhomogeneous state of competing COs has been suggested and a possible relation to the nonlinear conduction has been discussed.<sup>5,15–17)</sup> Although the present study is based on a uniform CO, we speculate that in a spatially nonuniform state, only domains of the horizontal CO are suppressed by an electric field, which results in nonlinear current-voltage characteristics similar to our results. The origin of the current oscillation in  $\theta$ -(ET)<sub>2</sub>X<sup>5)</sup> occurring with the nonlinear conduction is still unclear. However, Suko *et al.*<sup>6)</sup> have recently suggested that the oscillation is due to a current-induced

modulation of the lattice distortion, which may be related to our results.

In summary, we have investigated the mechanism of nonlinear conduction in  $\theta$ -(ET)<sub>2</sub>X. In the coexistent state of horizontal and 3-fold COs, the bias voltage weakens the lattice distortion and melts the horizontal CO. The metallic 3-fold CO remains even after the disappearance of the horizontal CO, which leads to selective melting of the latter CO. We have shown that these different responses depending on the spatial patterns of the two COs bring about the novel nonlinear conduction.

**Acknowledgments** This work was supported by Grants-in-Aid for Scientific Research (C) (Grant No. 23540426), Scientific Research (B) (Grant No. 20340101) and Scientific Research (A) (Grant No. 23244062), and by “Grand Challenges in Next-Generation Integrated Nanoscience” from the Ministry of Education, Culture, Sports, Science and Technology of Japan.

- 
- 1) G. Grüner: *Density Waves in Solids* (Addison-Wesley, Massachusetts, 1994).
  - 2) Y. Taguchi, T. Matsumoto, and Y. Tokura: Phys. Rev. B **62** (2000) 7015.
  - 3) S. Yamanouchi, Y. Taguchi, and Y. Tokura: Phys. Rev. Lett. **83** (1999) 5555.
  - 4) T. Oka, R. Arita, and H. Aoki: Phys. Rev. Lett. **91** (2003) 066406.
  - 5) F. Sawano, I. Terasaki, H. Mori, T. Mori, M. Watanabe, N. Ikeda, Y. Nogami, and Y. Noda: Nature **437** (2005) 522.
  - 6) T. Suko, I. Terasaki, H. Mori, and T. Mori: Materials **3** (2010) 2027.
  - 7) K. Miyagawa, A. Kawamoto, and K. Kanoda: Phys. Rev. B **62** (2000) R7679.
  - 8) R. Chiba, H. Yamamoto, K. Hiraki, T. Takahashi, and T. Nakamura: J. Phys. Chem. Solids **62** (2001) 389.
  - 9) H. Mori, S. Tanaka, and T. Mori: Phys. Rev. B **57** (1998) 12023.
  - 10) H. Tajima, S. Kyoden, H. Mori, and S. Tanaka: Phys. Rev. B **62** (2000) 9378.
  - 11) K. Yamamoto, K. Yakushi, K. Miyagawa, K. Kanoda, and A. Kawamoto: Phys. Rev. B **65** (2002) 085110.
  - 12) M. Watanabe, Y. Noda, Y. Nogami, and H. Mori: J. Phys. Soc. Jpn. **73** (2004) 116.
  - 13) M. Watanabe, Y. Nogami, K. Oshima, H. Mori, and S. Tanaka: J. Phys. Soc. Jpn. **68** (1999) 2654.
  - 14) Y. Nogami, J.-P. Pouget, M. Watanabe, K. Oshima, H. Mori, S. Tanaka, and T. Mori: Synth. Met. **103** (1999) 1911.
  - 15) T. Ito, M. Watanabe, K.-I. Yamamoto, N. Ikeda, Y. Nogami, Y. Noda, H. Mori, T. Mori, and I. Terasaki: Europhys. Lett. **84** (2008) 26002.
  - 16) T. S. Inada, I. Terasaki, H. Mori, and T. Mori: Phys. Rev. B **79** (2009) 165102.
  - 17) Y. Nogami, N. Hanasaki, M. Watanabe, K. Yamamoto, T. Ito, N. Ikeda, H. Ohsumi, H. Toyokawa, Y. Noda, I. Terasaki, H. Mori, and T. Mori: J. Phys. Soc. Jpn. **79** (2010) 044606.
  - 18) T. Mori, Y. Bando, T. Kawamoto, I. Terasaki, K. Takimiya, and T. Otsubo: Phys. Rev. Lett. **100** (2008) 037001.
  - 19) T. Mori, T. Ozawa, Y. Bando, T. Kawamoto, S. Niizeki, and H. Mori: Phys. Rev. B **79** (2009) 115108.
  - 20) H. Seo, C. Hotta, and H. Fukuyama: J. Phys. Soc. Jpn. **75** (2006) 051009.
  - 21) K. Kuroki: Sci. Tech. Adv. Mater. **10** (2009) 024312.
  - 22) Y. Tanaka and K. Yonemitsu: J. Phys. Soc. Jpn. **76** (2007) 053708.
  - 23) S. Miyashita and K. Yonemitsu: Phys. Rev. B **75** (2007) 245112.
  - 24) Y. Tanaka and K. Yonemitsu: J. Phys. Soc. Jpn. **77** (2008) 034708.

- 
- 25) T. Mori: J. Phys. Soc. Jpn. **72** (2003) 1469.  
26) M. Kaneko and M. Ogata: J. Phys. Soc. Jpn. **75** (2006) 014710.  
27) K. Yonemitsu: J. Phys. Soc. Jpn. **78** (2009) 054705.  
28) Y. Tanaka and K. Yonemitsu: Phys. Rev. B **83** (2011) 085113.  
29) M. Udagawa and Y. Motome: Phys. Rev. Lett. **98** (2007) 206405.